A Search for Faint Sources of Infrared Excess in the Spitzer Enhanced Imaging Products Catalog

1. NITARP Team

Educators:

- David Friedlander-Holm (The Bay School of San Francisco, San Francisco, CA)
- Nicholas Goeldi (Ripon High School, Ripon, WI)
- Matt Nowinski (Loudoun County Public Schools, Ashburn, VA and The Boeing Company)
- Alissa Sperling (Springside Chestnut Hill Academy, Philadelphia, PA)

Mentor Teacher:

- Thomas Rutherford (Sullivan South High School, Kingsport, TN)

Science Mentor:

- Varoujan Gorjian (Jet Propulsion Laboratory, Pasadena CA)

2. Abstract

The presence of infrared excess can be used to guide astronomers towards a wide range of short-lived, evolutionary galactic and extragalactic phenomena, such as young stellar objects, planet-forming regions around main sequence stars, and active galactic nuclei. This study searches the Spitzer Enhanced Imaging Products (SEIP) Catalog for sources of infrared excess. The SEIP contains 42 million point sources obtained by the Spitzer Space Telescope during its 5-year cryogenic mission. The SEIP is a unique repository of high resolution infrared data containing measurement of millions of objects were captured serendipitously in the field of view of the intended targets and have never been analyzed. This study continues the work of two previous efforts using color selection to produce a catalog of sources of infrared excess that can be used by astronomers for follow-up analysis and observations aimed at improving our understanding of stellar and galactic evolution. In an effort to improve the robustness of the resulting catalog, this work will apply filtering options available in the SEIP that minimize contamination by nearby saturated sources and/or crowded fields. In addition, this research will focus on fainter sources (magnitude ≥ 8 at 24 μm), which should reveal a number of new sources of infrared excess not detectable by previous infrared surveys, such as the Wide-Field Infrared Survey Explorer (WISE).

3. Background

Stars, galaxies, and other astronomical objects essentially behave as if they are blackbodies. Most astronomical objects emit energy in the form of electromagnetic radiation according to their temperatures. From the high energy gamma rays emitted by neutron stars and pulsars to the dust-surrounded quasars emitting low frequency radio waves, the electromagnetic radiation given off by an object can tell us much about its composition and life cycle. The wavelength at which the greatest energy output occurs is denoted as λ_{max}. As illustrated in Figure 1, when emitted energy is plotted versus wavelength, both the value of λ_{max} and the area under the curve vary according to the temperature of the object. The shape of these "blackbody" radiation curves is composed of two parts: (1) the Wien Displacement Law, which

defines the shape of the left part of the curve and λ_{max}; and (2) the Rayleigh-Jeans Law, which defines the right part of the blackbody curve.

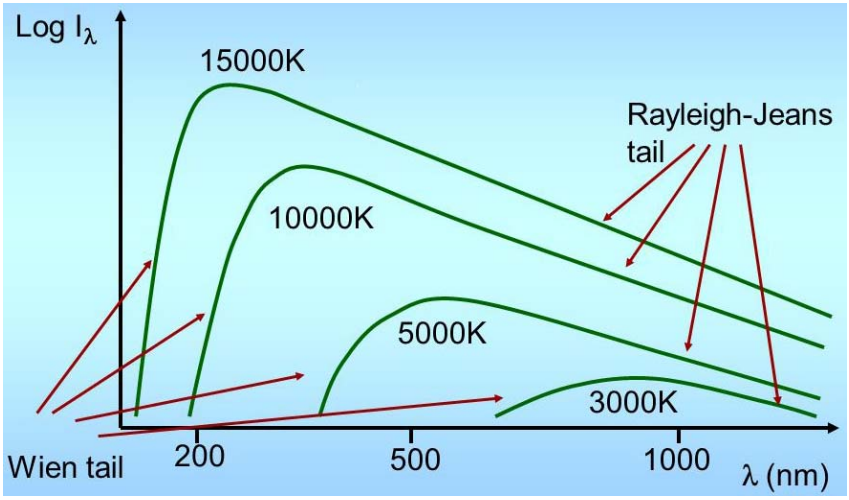

Figure 1. Blackbody radiation curves for a range of temperatures. The Wien (left) and Rayleigh-Jeans (right) components of the curves are indicated by the red arrows.

Infrared excess is a term used to describe the measurement of an astronomical source of light, such as a star or galaxy, which exhibits additional spectral energy in the infrared wavelength range as compared to the standard blackbody radiation curve. The presence of infrared excess is an indicator of nearby dust that is being heated by an energetic object. An example of infrared excess is provided in Figure 2. This diagram illustrates how the presence of a dust disk or a dust belt around a star produces excess energy at infrared wavelengths relative to that produced by the star alone. In these cases, the energy of the star is absorbed by the surrounding dust and re-emitted primarily in the infrared range.

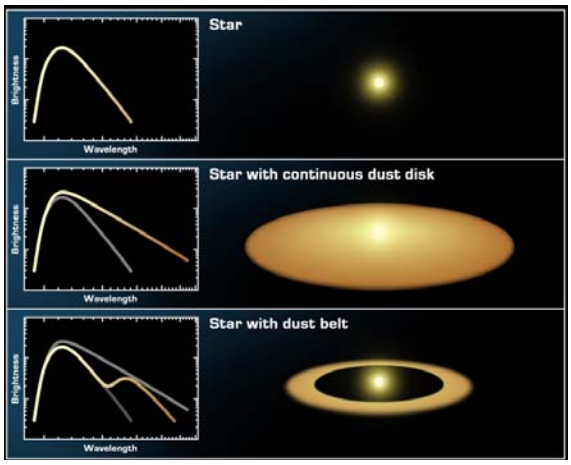

Figure 2. Stellar infrared excess due to a dust disk or belt (Pyle, 2005). The top graphic illustrates the ideal blackbody emissions of an isolated star. The middle graphic shows the infrared excess generated by a continuous disk of dust around the star. The bottom graphic illustrates the infrared excess generated by a star with a dust belt.

There are several different potential sources of infrared excess, including young stellar objects (YSO), evolved low- to intermediate-mass stars, active galactic nuclei (AGN), luminous infrared galaxies (LIRG), and main sequence stars with dusty disks or belts. These sources are described briefly in the following sections.

3.1. Sources of Infrared Excess

3.1.1. Young Stellar Objects

Stars are formed when molecular clouds contract and compress due the gravitational attraction of gas and dust particles. This contraction can be triggered by radiation pressure from nearby stars, density fluctuations in the interstellar medium, or shock waves from supernovae or other events. As the gas and dust cloud collapses, pressure begins to build at the center of the young star and radiation is released. The term "young stellar object" refers to this early evolutionary stage of stars and is categorized into different classes (Class 0, I, II, III) according to the respective spectral energy distribution (SED) (Lada, 1987; MacGregor, 2013). Each of the classes of YSO's exhibits different levels of infrared excess according to the amount and arrangement of dust around the forming star. As shown in Figure 3, as the star evolves, the surrounding dust transitions from circumstellar envelope (Class 0) to primordial disk (Class I and II) to debris field (Class III). Each of these stages is associated with a characteristic SED.

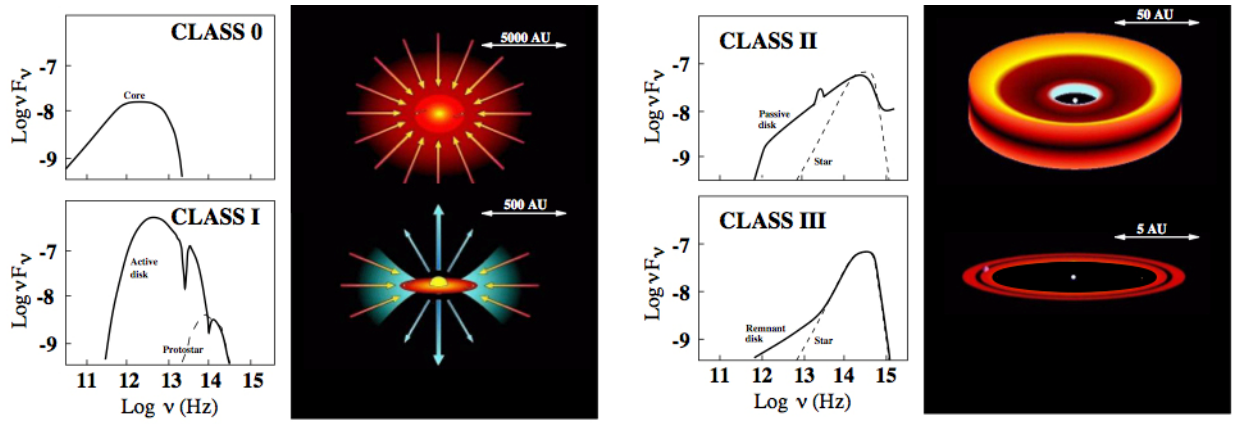

Figure 3. Spectral energy distribution of a YSO (adapted from Isella, 2006). The four evolutionary YSO stages, Class 0, I, II, and III, are shown. The x-axis of the SED plots is the logarithm of the frequency of the emitted light.

3.1.2. Evolved Stars

Evolved, low- to intermediate-mass stars enter a "superwind" phase at the end of their time on the asymptotic giant branch (AGB) of the Hertzsprung-Russell (HR) diagram. During this phase, these so-called post-AGB stars eject from 20 to 80 percent of their mass. As the ejected material cools, some of it is condensed into dust (Wallerstein and Knapp, 1998). The shorter wavelength energy emitted by the central star is absorbed by the ejected dust and re-emitted at longer wavelengths in the infrared. An example of a post-AGB star is shown in Figure 4. The Infrared Astronomical Satellite (IRAS) mission measured a large surplus of infrared light from HD101584 as a result of the dust that was blown off during the superwind phase.

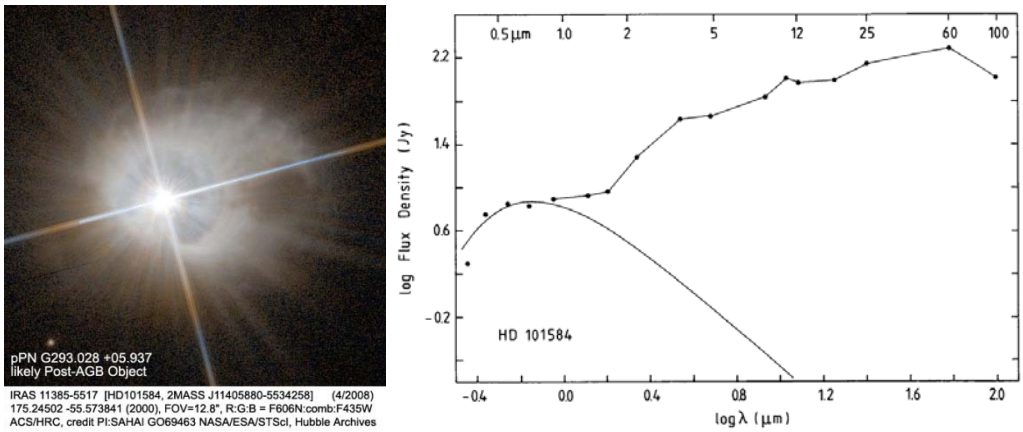

Figure 4. Hubble image (left) and flux density distribution (right) (Parthasarathy and Pottasch, 1986) of the post-AGB star, HD101584. The solid line curve at the lower left of the plot is the blackbody curve.

3.1.3. Active Galactic Nuclei

Similar to Sagittarius A* at the center of our own Milky Way galaxy, it is believed that a supermassive black hole exists at the center of each galaxy in the universe. The supermassive black hole may accrete gas from the surrounding galaxy, forming a high-temperature disk. The SED of this accretion disk can be approximated by a superposition of blackbody radiation curves peaking at ultraviolet wavelengths. This energy, however, is re-absorbed by a torus of dusty material which surrounds the galaxy and is re-emitted in the infrared (Antonucci, 1993). This infrared excess distinguishes AGN from normal, non-active galaxies. An example of the SED of an AGN and its constituent components is shown in Figure 5.

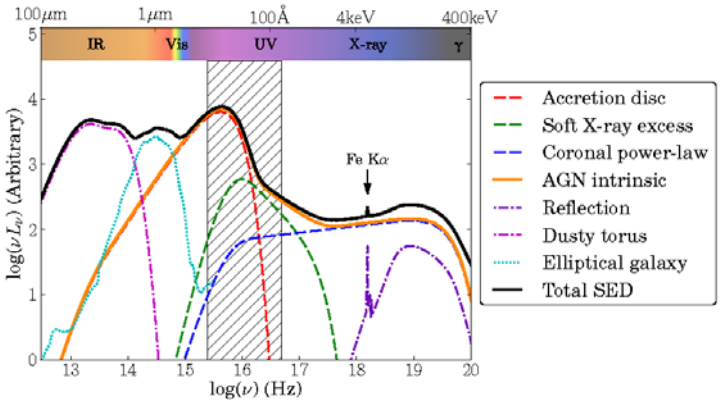

Figure 5. Spectral energy distribution of an active galactic nucleus. The contributions of the accretion disk (dotted red line) and dusty torus (dotted magenta line) are also shown (Collinson et al., 2017).

3.1.4. Luminous Infra-Red Galaxies

As galaxies move through space they interact and collide with each other. The energy emitted by such interactions is generated by a combination of the core active galactic nuclei and the very high rate of new star formation associated with the early stages of these galactic collisions. This energy is absorbed by dust within the colliding galaxies and re-emitted in the infrared

(Joseph and Wright, 1985). Such extragalactic sources of infrared excess are commonly referred to as Luminous Infra-Red Galaxies (LIRG). The most luminous of these sources are called ultraluminous (ULIRG) or hyperluminous (HyLIRG) infrared galaxies. The presence of infrared excess distinguishes LIRG, ULIRG, and HyLIRG from normal, non-active galaxies. As an example of an LIRG, Figure 6 provides multispectral imagery and the flux density distribution for the interacting galaxy II ZW 096.

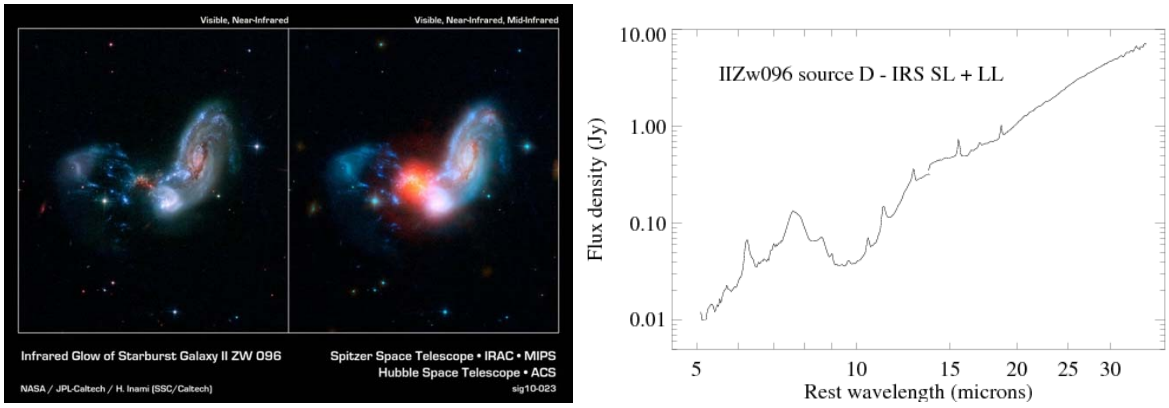

Figure 6. Multispectral Hubble and Spitzer images (left) and Spitzer Infrared Spectrograph (IRS) flux density distribution (right) for the interacting galaxy II Zw 096 (Inami et al., 2010).

3.1.5. Main Sequence Debris Disks

The Sun is surrounded by planets, dust, asteroids, and other forms of leftover debris from the formation of our solar system. All of these objects absorb light from the Sun and re-emit it in the infrared. Like the Sun, many main sequence stars have debris disks produced by comet evaporation or asteroid collisions and produce infrared excess. Such warm, dusty circumstellar regions (T = 150 to 200 K) could provide insight into the formation and evolution of our own planet and solar system (Werner et al., 2006; Wyatt, 2008). A combination of Spitzer, WISE, and AKARI data has been used to identify approximately 500 stellar debris disks with warm dust components (Vican and Schneider, 2013; Morales et al., 2011; Ishihara et al., 2017; and others). An example of a main sequence star with a debris belt is provided in Figure 7 for Vega.

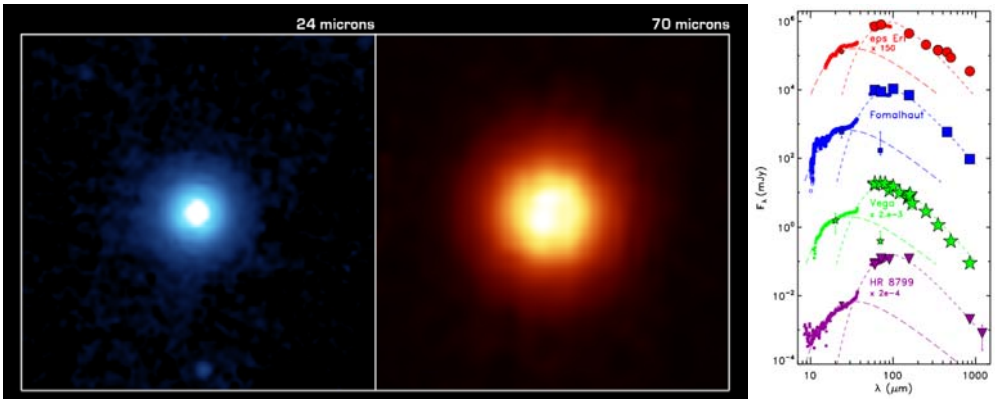

Figure 7. Spitzer MIPS (24 and 70 μm) imagery (left) and spectral energy distribution (right, green points) (Su et al., 2013) of the Vega debris disk.

3.2. Identifying Infrared Excess

The previously described examples of infrared excess demonstrate how these sources can be identified by looking for deviations from the theoretical blackbody radiation curve in the infrared wavelength range. As shown in Figure 8, wavelengths longer than the peak of the blackbody curve, referred to as the Rayleigh-Jeans line, are characterized by a constant, temperature-independent slope. This slope can be quantitatively described by one or more "colors," defined as the ratio in flux for two distinct wavelengths. In practice, these colors are calculated from the infrared channels provided by a given infrared instrument (e.g., Spitzer IRAC I1-I4 (3.6, 4.5, 5.8, 8.0 µm) or MIPS M1 (24 µm)).

A color-color diagram (CCD), like the one shown in Figure 9, plots a pair of colors for several sources and is an effective method of identifying sources that have infrared excess. In this diagram, objects which do not exhibit infrared excess will cluster near zero (i.e. in Figure 9, [3.6]-[4.5] = 0 and [4.5]-[24] = 0), an indication that their spectral energy distribution is close to that of a blackbody. Objects which do exhibit infrared excess will tend to populate the region to the upper right. For the current study, color-color diagrams will be used to identify sources of infrared excess in the SEIP catalog that deviate significantly from the main locus of points.

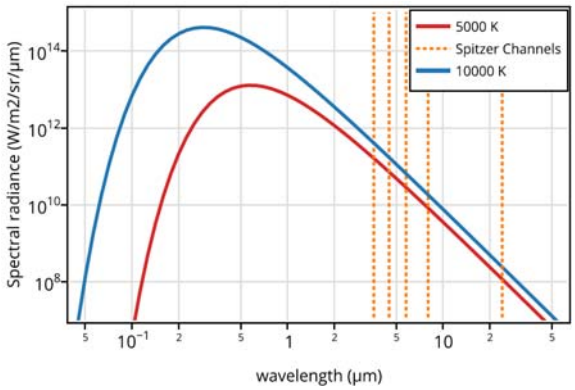

Figure 8. Blackbody radiation curves for temperatures of 5000 K and 10000 K. The four IRAC channels (I1, I2, I3, I4; 3.6, 4.5, 5.8, 8.0 µm) and MIPS M1 channel (24 µm) are indicated by the vertical red dotted lines (Strasburger et al., 2015).

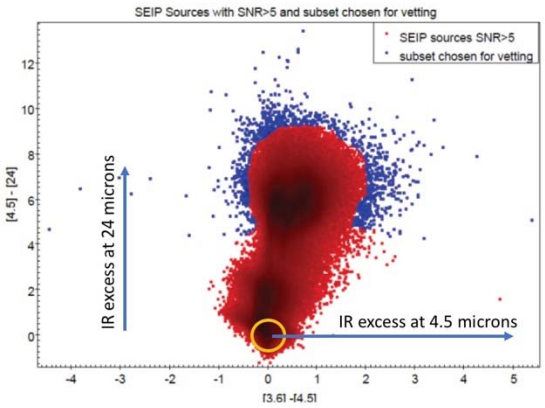

Figure 9. Color-Color Diagram from the SEIP Catalog using Spitzer IRAC I1-I2 (3.6 µm - 4.5 µm) and IRAC I2-MIPS M1 (4.5 µm - 24 µm) (Rowe et al., 2018). The orange circle denotes sources near zero-zero that have a blackbody spectrum with no IR excess.

3.3. Spitzer Enhanced Imaging Products Catalog

The Spitzer Enhanced Imaging Products (SEIP) catalog (Teplitz et al., 2012) is comprised of all images taken during Spitzer's 5-year cryogenic mission. Data are available from Channels I1 through I4 (3.6, 4.5, 5.8, and 8 µm) of the Infrared Array Camera (IRAC) and Channel M1 (24 µm) of the Multiband Imager and Photometer for Spitzer (MIPS). The SEIP database includes both Super Mosaics (combinations of multiple observing frames) and a Source List of photometry for compact sources. The SEIP Source List was constructed with a priority on high reliability; with coverage, completeness, and limiting magnitude being secondary considerations. In total, the SEIP catalog encompasses images of approximately 42 million different point sources, many of which were incidental observations included in the field of view of the intended target. Hence, the SEIP catalog potentially contains millions of targets which have yet to be studied and represents a unique opportunity to discover new sources of infrared excess.

Relative to other infrared catalogs, the SEIP provides significant advantages in both sensitivity and spatial resolution. As an example, compared to the Wide-Field Infrared Survey Explorer (WISE), Spitzer provides more than two times the resolution across similar infrared bands. This improved resolution makes the SEIP less susceptible to the false identification of infrared excess due to nearby sources, such as unresolved companion stars. Spitzer also provides improved sensitivity over WISE, as illustrated in Figure 10 for the 22 (W4) and 24 (M1) µm wavelengths. From this plot, it can be seen that the sensitivity of WISE W4 channel drops off rapidly beyond a magnitude of 8. Since the Spitzer observations were not part of a uniform survey with a single exposure time, there is no distinct roll-off of sensitivity as there is for the uniform WISE survey and the sensitivity of the Spitzer MIPS M1 channel remains relatively flat through a magnitude of 11. This magnitude difference represents an effective improvement of sensitivity for Spitzer (over WISE) of more than 3 times, resulting in increased detection of extragalactic and faint galactic infrared sources.

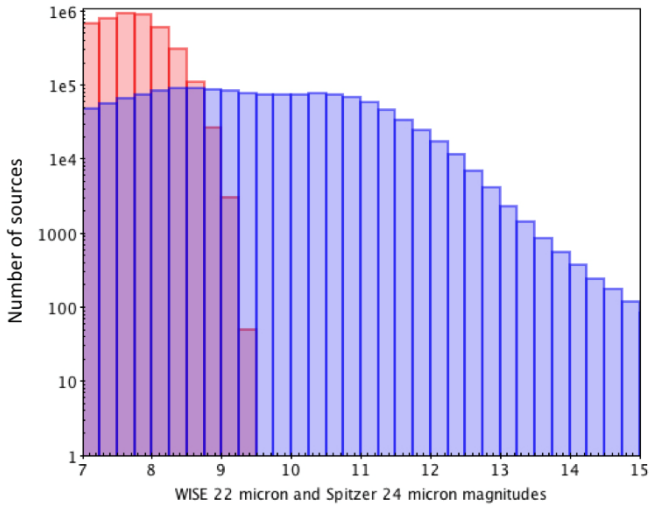

Figure 10. Comparison of instrument sensitivity of the SEIP MIPS M1 Channel (24 µm) (blue) and the WISE W4 Channel (22 µm) (Red) for S/N ≥ 5 (Gorjian, 2018)

Two previous studies have used color-color diagrams, based on IRAC Bands I1, I2, and MIPS M1, to identify sources of infrared excess in the SEIP catalog. The overall objective of these studies was to produce a catalog of infrared excess sources which astronomers could use to perform follow-up observations and analyses of the phenomena described in Section 3.1.

Strasburger et al. (2015) considered SEIP sources which had a signal-to-noise ratio (S/N) of 10 or more in all bands. In addition, they ignored objects that were from "highly studied regions", including the galactic plane and those areas of the sky observed by other infrared surveys. From the resulting set of sources, color-color diagram "outliers" were identified and the associated images were manually analyzed to exclude any sources which may have been incorrectly cross-matched (i.e. IRAC and MIPS band data was not from the same source) or whose photometric values have been contaminated by image artifacts or nearby bright sources. In total, Strasburger et al. (2015) identified 90 verified sources of infrared excess. Of these, 76 objects were determined to be newly discovered.

Rowe et al. (2018) extended the work of Strasburger et al. (2015) with the primary goal to "…dig deeper into the [SEIP] catalog in an attempt to find more IRXS [infrared excess] sources." This study expanded the initial data set by considering SEIP sources which had S/N of 5 or more in all bands, yielding a total of approximately 461,000 sources. A set of 985 "interesting" targets was identified by selecting the most extreme examples of excess in the MIPS M1 band from the color-color diagram (see blue points in Figure 9). A visual inspection of the associated images yielded 512 verified sources of infrared excess. Of these, 346 were determined to be newly discovered. Based on the IRAC I1 magnitude, 98 of these were identified as likely galactic sources and 248 as likely extragalactic sources.

The following section describes in detail how this study will improve upon these previous efforts.

4. Science

4.1. Objectives

This work will extend and refine the work of Strasburger et al. (2015) and Rowe et al. (2018) to identify infrared sources in the SEIP catalog. Specifically, this study will make use of criteria available in the SEIP database to improve the accuracy of infrared excess source detection and to minimize the time required for manual verification of the associated images. In addition, in an effort to avoid duplication with infrared excess sources previously identified by WISE, only sources with a magnitude of 8 (defined by MIPS M1) or fainter will be considered.

4.2. Method

The analytical method employed by this effort is described below:

1. Filter the SEIP catalog sources using the following criteria:
    a. S/N ≥ 5 for IRAC I1 (3.6 μm), I2 (5.6 μm), and MIPS M1 (24 μm)
    b. **FluxFlag* = 0 for IRAC channels I1 and I2 (minimizes number of sources whose flux density in the IRAC bands may be affected by nearby saturated or extended objects)

   c. **M1_BrtFrac* < 0.5 and **M1_ExtFrac* < 0.5 (minimizes number of sources whose flux density in the MIPS M1 band may be affected by nearby saturated or extended objects)
   d. MIPS M1 magnitude ≥ 8
2. Generate [I2-M1] vs [I1-I2] color-color diagrams (CCD) from the approximately 360,000 available sources identified in Step 1 using the Tool for OPerations on Catalogues And Tables (TOPCAT) software. The color-color diagrams will be used to identify sources with infrared excess
3. Ensure the validity of sources showing MIPS M1 infrared excess by visually inspecting the associated IRAC I1, I2, and M1 images. This is required due to the potential presence of image artifacts or saturation, and because the SEIP catalog may not have accurate source matching across wavelengths leading to incorrect matches between the lower resolution M1 24 um and the higher resolution I1 and I2 images
4. Categorize the remaining sources as galactic (IRAC I1 magnitude < 14) or extragalactic (IRAC I1 magnitude ≥ 14) (Strasburger et al., 2015)
5. Identify new sources of infrared excess by eliminating any objects which have already been identified as sources of infrared excess in the Set of Identifications, Measurements, and Bibliography for Astronomical Data (SIMBAD)
6. Produce a final catalog of infrared excess objects for follow-up analyses and observations

4.3. Expected Outcomes

In keeping with the previous work conducted by Strasburger et al. (2015) and Rowe et al. (2018), the primary objective of this study is to generate a catalog of infrared excess sources from the SEIP catalog. By employing SEIP database filter criteria (**FluxFlag, *M1_BrtFrac*, and **M1_ExtFrac*), it is expected that this study will identify a more robust set of infrared excess sources that will contain a significantly smaller number of false positives. In addition, by limiting potential sources to MIPS M1 magnitudes of 8 or fainter, it is anticipated that sources of infrared excess will be found that were undetected due to the sensitivity limitations of WISE. It is likely that a large percentage of these objects identified will be extragalactic rather than galactic. The final catalog produced by this study will comprise a reliable set of sources of infrared excess which can be used by astronomers for additional analysis and/or follow-up observations to improve our knowledge of stellar/galactic formation and evolution.

4.4. Data and Tools

This study is principally based on data from the SEIP catalog. However, to help further characterize specific objects showing promising infrared excess, visible and near-infrared data from additional databases may be used. These include SIMBAD, Two Micron All-Sky Survey (2MASS), the NASA/IPAC Extragalactic Database (NED), the Palomar Observatory Sky Survey (POSS), and the Sloan Digital Sky Survey (SDSS). Processing of the astronomical data will be performed using TopCat. The visual inspection and source verification of SEIP imagery will be performed using IRSA Visualization Tool.

5. Education

5.1. Research

The educational component of the project tracks both astronomy content knowledge and perceptions of science and scientific research for secondary students over the course of a calendar year. This project will be carried out by the educator members of the NITARP team. The NITARP student participants and other students in the target schools will be assessed in February 2018 and then again in November 2018. Students' answers to questions will be correlated to their current academic science placement and to participation in the NITARP program. To determine astronomy content knowledge, students will be given an electronic version of the Test of Astronomy Standards (TOAST), a metric designed by S. Slater at the Center for Astronomy and Physics Education Research. TOAST asks content-based questions at an introductory undergraduate level. To assess attitudes and perceptions of science and scientific research, students will be given an electronic version of the Views on Science and Education Questionnaire (VOSE). VOSE was created by S. Chen at the National Taiwan University of Science and Technology and asks students to rate the merit of scientific pursuits and goals on a relative scale. The combined education research questionnaires provided to students should take about 40 minutes to complete and will be administered by the NITARP teachers pending institutional approval. Although names and other identifying demographic information will be collected for each student at the completion of the assessments, it will only be used to correlate pre- and post-year data and will be removed from the final research. The results of these surveys will be presented during the 233rd meeting of the American Astronomical Society (AAS) in Seattle, WA.

5.2. Outreach

David Friedlander-Holm (The Bay School of San Francisco, San Francisco, CA)

- Run a course for California teachers through the California Teacher Development Collaborative (CATDC) on the importance, benefits of, and methods for involving students in science research
- Present to the San Francisco Amateur Astronomers on our research methods and outcomes
- Incorporate research methods and tools into Bay courses, starting with the Astronomy & Astrophysics courses
- Share findings with Science department
- Present to various middle and high school teachers as opportunities arise

Nicholas Goeldi (Ripon High School, Ripon, WI):

- Present our work to the Phox Valley Share group & NSTA
- Redesign the Ripon Astronomy and Astrophysics curriculum to be more research-based
- Help provide students with a more authentic astronomy experience
- Present to the school board about the NITARP experience
- Presentation at the 2019 National NSTA meeting in St. Louis, MO

Matt Nowinski (Loudoun County Public Schools, Ashburn, VA and the Boeing Company):

- In coordination with Loudoun County Public Schools Department of Human Resources and Talent Development (HRTD) Office, organize and conduct county-wide research-centered workshops for science teachers during the 2018-2019 school year
- Organize and conduct a similar set of workshops in my local LCPS schools: Algonkian Elementary Schools, River Bend Middle School, and Potomac Falls High School. Follow-up regularly with participant teachers as part of my current series of in-classroom STEM lessons
- Incorporate NITARP experience and materials during in-school, after-school, and summer STEM volunteer activities

Alissa Sperling (Springside Chestnut Hill Academy, Philadelphia, PA)

- Bring NITARP students to the Springside Chestnut Hill Academy Middle School "star parties" to educate young students about astronomy research
- Host a table at The Franklin Institute Science Museum "Science After Hours" event to present NITARP research
- Run a professional development seminar on incorporating student research into the classroom for Philadelphia area teachers
- Present to the local AAPT chapter about student research experiences

Tom Rutherford (Sullivan South High School, Kingsport, TN)

- Presentation at the 2019 National NSTA meeting in St. Louis, MO
- Public presentation to the Bays Mountain Astronomy Club, Bays Mountain Park and Planetarium, Kingsport, Tennessee
- Presentation at the East Tennessee State University (ETSU) Physics Seminar
- Presentation before the ETSU College of Education teacher candidates
- Presentation before the King University College of Education teacher candidates
- Presentation before the Milligan College teacher candidates
- Staff development session before the school district teachers
- Poster presentation at the 2019 American Astronomical Society meeting in Seattle, WA
- Interviews with local television stations and newspapers
- Classroom application of what I learn about using large NASA databases and data analysis with my Astronomy classes at the high school where I teach
- Other venues as the opportunity arises

References

Antonucci, R., 1993. Unified models for active galactic nuclei and quasars. \araa 31, 473–521. https://doi.org/10.1146/annurev.aa.31.090193.002353

Collinson, J.S., Ward, M.J., Landt, H., Done, C., Elvis, M., McDowell, J.C., 2017. Reaching the peak of the quasar spectral energy distribution - II. Exploring the accretion disc, dusty torus and host galaxy. \mnras 465, 358–382. https://doi.org/10.1093/mnras/stw2666

Gorjian, V., 2018. SEIP WISE 22-24um Comparison. Pers. Commun.

Greene, T.P., Wilking, B.A., Andre, P., Young, E.T., Lada, C.J., 1994. Further mid-infrared study of the rho Ophiuchi cloud young stellar population: Luminosities and masses of pre-main-sequence stars. \apj 434, 614–626. https://doi.org/10.1086/174763

Inami, H., Armus, L., Surace, J.A., Mazzarella, J.M., Evans, A.S., Sanders, D.B., Howell, J.H., Petric, A., Vavilkin, T., Iwasawa, K., Haan, S., Murphy, E.J., Stierwalt, S., Appleton, P.N., Barnes, J.E., Bothun, G., Bridge, C.R., Chan, B., Charmandaris, V., Frayer, D.T., Kewley, L.J., Kim, D.C., Lord, S., Madore, B.F., Marshall, J.A., Matsuhara, H., Melbourne, J.E., Rich, J., Schulz, B., Spoon, H.W.W., Sturm, E., U, V., Veilleux, S., Xu, K., 2010. The Buried Starburst in the Interacting Galaxy II Zw 096 as Revealed by the Spitzer Space Telescope. \aj 140, 63–74. https://doi.org/10.1088/0004-6256/140/1/63

Isella, A., 2006. Interferometric observations of pre-main sequence disks. Universit`a degli Studi di Milano, Milano, Italy.

Ishihara, D., Takeuchi, Nami, Kobayashi, Hiroshi, Nagayama, Takahiro, Kaneda, Hidehiro, Inutsuka, Shu-ichiro, Fujiwara, Hideaki, Onaka, Takashi, 2017. Faint warm debris disks around nearby bright stars explored by AKARI and IRSF⋆. A&A 601, A72. https://doi.org/10.1051/0004-6361/201526215

Joseph, R.D., Wright, G.S., 1985. Recent star formation in interacting galaxies. II - Super starburst in merging galaxies. \mnras 214, 87–95. https://doi.org/10.1093/mnras/214.2.87

Lada, C.J., 1987. Star formation - From OB associations to protostars, in: Peimbert, M., Jugaku, J. (Eds.), Star Forming Regions, IAU Symposium. pp. 1–17.

MacGregor, M., 2013. Interpreting Spectral Energy Distributions from Young Stellar Objects. ISM Star Form.

Morales, F.Y., Rieke, G.H., Werner, M.W., Bryden, G., Stapelfeldt, K.R., Su, K.Y.L., 2011. Common Warm Dust Temperatures Around Main-sequence Stars. \apjl 730, L29. https://doi.org/10.1088/2041-8205/730/2/L29

Parthasarathy, M., Pottasch, S.R., 1986. The far-infrared (IRAS) excess in HD 161796 and related stars. \aap 154, L16–L19.

Pyle, T., 2005. The Invisible Disk [WWW Document]. Invis. Disk. URL http://www.spitzer.caltech.edu/images/2632-sig05-026-The-Invisible-Disk

Rowe, J.L., Duranko, G., Gorjian, V., Lineberger, H., Orr, L., Adewole, A., Bradford, E., Douglas, A., Kohl, S., Larson, L., Lascola, G., Orr, Q., Scott, M., Walston, J., Wang, X., 2018. A Search to Uncover the Infrared Excess (IRXS) Sources in the Spitzer Enhanced Imaging Products (SEIP) Catalog. Presented at the American Astronomical Society Meeting Abstracts #231, p. #151.02.

Strasburger, D., Gorjian, V., Burke, T., Childs, L., Odden, C., Tambara, K., Abate, A., Akhtar, N., Beach, S., Bhojwani, I., Brown, C., Dear, A., Dumont, T., Harden, O., Joli-Coeur, L., Nahirny, R., Nakahira, A., Nix, S., Orgul, S., Parry, J., Picken, J., Taylor, I., Toner, E., Turner, A., Xu, J., Zhu, E., 2015. Identification and Classification of Infrared Excess Sources in the Spitzer Enhanced Imaging Products (SEIP) Catalog. Presented at the American Astronomical Society Meeting Abstracts #225, p. 336.26.

Su, K.Y.L., Rieke, G.H., Malhotra, R., Stapelfeldt, K.R., Hughes, A.M., Bonsor, A., Wilner, D.J., Balog, Z., Watson, D.M., Werner, M.W., Misselt, K.A., 2013. Asteroid Belts in Debris Disk Twins: Vega and Fomalhaut. \apj 763, 118. https://doi.org/10.1088/0004-637X/763/2/118

Teplitz, H.I., Capak, P., Hanish, D., Brooke, T.Y., Colbert, J.W., Desai, V., Hoard, D.W., Howell, J., Laher, R., Noriega-Crespo, A., 2012. Spitzer Heritage Archive Enhanced Imaging Products, in: American Astronomical Society Meeting Abstracts #219, American Astronomical Society Meeting Abstracts. p. 428.06.

Vican, L., Schneider, A., 2013. THE EVOLUTION OF DUSTY DEBRIS DISKS AROUND SOLAR TYPE STARS. Astrophys. J. 780, 154. https://doi.org/10.1088/0004-637X/780/2/154

Wallerstein, G., Knapp, G.R., 1998. Carbon Stars. \araa 36, 369–434. https://doi.org/10.1146/annurev.astro.36.1.369

Werner, M., Fazio, G., Rieke, G., Roellig, T.L., Watson, D.M., 2006. First Fruits of the Spitzer Space Telescope: Galactic and Solar System Studies. Annu. Rev. Astron. Astrophys. 44, 269–321. https://doi.org/10.1146/annurev.astro.44.051905.092544

Wyatt, M.C., 2008. Evolution of Debris Disks. Annu. Rev. Astron. Astrophys. 46, 339–383. https://doi.org/10.1146/annurev.astro.45.051806.110525

Links

2MASS:	https://www.ipac.caltech.edu/2mass/
POSS:	http://cas.sdss.org/dr7/en/proj/advanced/skysurveys/poss.asp
SDSS:	http://www.sdss.org/
SEIP:	https://irsa.ipac.caltech.edu/data/SPITZER/Enhanced/SEIP
SIMBAD:	http://simbad.u-strasbg.fr/simbad/
TopCat:	http://www.star.bris.ac.uk/~mbt/topcat/